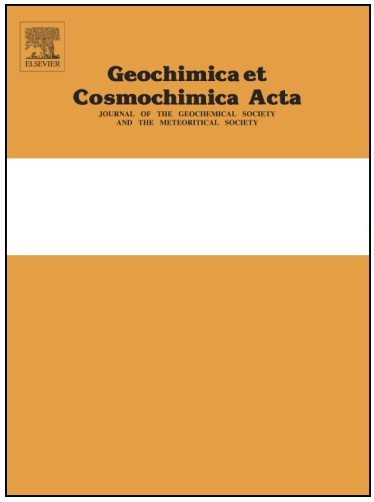

The Phanerozoic δ $^{88/86}$Sr Record of Seawater: New Constraints on Past Changes in Oceanic Carbonate Fluxes

Hauke Vollstaedt, Anton Eisenhauer, Klaus Wallmann, Florian Böhm, Jan Fietzke, Volker Liebetrau, André Krabbenhöft, Juraj Farkaš, Adam Tomašových, Jacek Raddatz, Ján Veizer

PII: S0016-7037(13)00562-0
DOI: http://dx.doi.org/10.1016/j.gca.2013.10.006
Reference: GCA 8484

To appear in: *Geochimica et Cosmochimica Acta*

Received Date: 16 April 2013
Accepted Date: 3 October 2013

Please cite this article as: Vollstaedt, H., Eisenhauer, A., Wallmann, K., Böhm, F., Fietzke, J., Liebetrau, V., Krabbenhöft, A., Farkaš, J., Tomašových, A., Raddatz, J., Veizer, J., The Phanerozoic δ $^{88/86}$Sr Record of Seawater: New Constraints on Past Changes in Oceanic Carbonate Fluxes, *Geochimica et Cosmochimica Acta* (2013), doi: http://dx.doi.org/10.1016/j.gca.2013.10.006

The Phanerozoic $\delta^{88/86}Sr$ Record of Seawater: New Constraints on Past Changes in Oceanic Carbonate Fluxes

Hauke Vollstaedt[a,1,*], Anton Eisenhauer[a], Klaus Wallmann[a], Florian Böhm[a], Jan Fietzke[a], Volker Liebetrau[a], André Krabbenhöft[a,2], Juraj Farkaš[b,c], Adam Tomašových[d], Jacek Raddatz[a], and Ján Veizer[e]

[a] GEOMAR, Helmholtz-Zentrum für Ozeanforschung Kiel, Wischhofstr. 1-3, 24148 Kiel, Germany
[b] Department of Geochemistry, Czech Geological Survey, Geologická 6, 152 00 Prague 5, Czech Republic
[c] Department of Environmental Geosciences, Czech University of Life Sciences, Kamýcká 129, 165 21 Prague 6, Czech Republic
[d] Department of Geophysical Sciences, The University of Chicago, 5734 S Ellis Ave., IL 30367, Chicago, USA
[e] Ottawa-Carleton Geoscience Center, University of Ottawa, Ottawa ON K1N 6N5, Canada

Abstract

The isotopic composition of Phanerozoic marine sediments provides important information about changes in seawater chemistry. In particular, the radiogenic strontium isotope ($^{87}Sr/^{86}Sr$) system is a powerful tool for constraining plate tectonic processes and their influence on atmospheric CO_2 concentrations. However, the $^{87}Sr/^{86}Sr$ isotope ratio of seawater is not sensitive to temporal changes in the marine strontium (Sr) output flux, which is primarily controlled by the burial of calcium carbonate ($CaCO_3$) at the ocean floor. The Sr budget of the Phanerozoic ocean, including the associated changes in the amount of $CaCO_3$ burial, is therefore only poorly constrained. Here, we present the first stable isotope record of Sr for Phanerozoic skeletal carbonates, and by inference for Phanerozoic seawater ($\delta^{88/86}Sr_{sw}$), which we find to be sensitive to imbalances in the Sr input and output fluxes. This $\delta^{88/86}Sr_{sw}$ record varies from ~0.25‰ to ~0.60‰ (vs. SRM987) with a mean of ~0.37‰. The fractionation factor between modern seawater and skeletal

[1] Present address: Center for Space and Habitability + Institut für Geologie, Universität Bern, Baltzerstrasse 1 + 3, 3012 Bern, Switzerland
[2] Present address: Leyegasse 4, 69117 Heidelberg, Germany
* Corresponding author. Phone: +41 31 631 8533, fax: +41 31 631 4843

E-mail addresses: hauke.vollstaedt@csh.unibe.ch (H. Vollstaedt), aeisenhauer@geomar.de (A. Eisenhauer), kwallmann@geomar.de (K. Wallmann), fboehm@geomar.de (F. Böhm), jfietzke@geomar.de (J. Fietzke), vliebetrau@geomar.de (V. Liebetrau), Andre.Krabbenhoeft@tesa.com (A. Krabbenhöft), juraj.farkas@gelogy.cz (J. Farkaš), Adam.Tomasovych@savba.sk (A. Tomašových), jraddatz@geomar.de (J. Raddatz), jveizer@uottawa.ca (J. Veizer)

calcite $\Delta^{88/86}Sr_{cc\text{-}sw}$, based on the analysis of 13 modern brachiopods (mean $\delta^{88/86}Sr$ of 0.176±0.016‰, 2 standard deviations (s.d.)), is -0.21‰ and was found to be independent of species, water temperature, and habitat location. Overall, the Phanerozoic $\delta^{88/86}Sr_{sw}$ record is positively correlated with the Ca isotope record ($\delta^{44/40}Ca_{sw}$), but not with the radiogenic Sr isotope record ($(^{87}Sr/^{86}Sr)_{sw}$). A new numerical modeling approach, which considers both $\delta^{88/86}Sr_{sw}$ and $(^{87}Sr/^{86}Sr)_{sw}$, yields improved estimates for Phanerozoic fluxes and concentrations for seawater Sr. The oceanic net carbonate flux of Sr ($F(Sr)_{carb}$) varied between an output of $-4.7x10^{10}$mol/Myr and an input of $+2.3x10^{10}$mol/Myr with a mean of $-1.6x10^{10}$mol/Myr. On time scales in excess of 100Myrs the $F(Sr)_{carb}$ is proposed to have been controlled by the relative importance of calcium carbonate precipitates during the “aragonite” and “calcite” sea episodes. On time scales less than 20Myrs the $F(Sr)_{carb}$ seems to be controlled by variable combinations of carbonate burial rate, shelf carbonate weathering and recrystallization, ocean acidification, and ocean anoxia. In particular, the Permian/Triassic transition is marked by a prominent positive $\delta^{88/86}Sr_{sw}$-peak that reflects a significantly enhanced burial flux of Sr and carbonate, likely driven by bacterial sulfate reduction (BSR) and the related alkalinity production in deeper anoxic waters. We also argue that the residence time of Sr in the Phanerozoic ocean ranged from ~1Myrs to ~20Myrs.

1 Introduction

The continental weathering of silicate rocks is probably the most important sink for atmospheric CO_2 and therefore one of the dominant processes that controls climate on geological time scales (Berner and Berner, 2012; Berner, 1994; Gaillardet et al., 1999; Kothavala et al., 1999). In order to reconstruct atmospheric CO_2 through Earth`s history, the radiogenic isotope systems, such as Re/Os and Rb/Sr, serve as powerful tools because they provide information about the past dynamics of continental weathering and its interaction with atmospheric pCO_2.

Sr has a residence time of 2.5Myrs (Hodell et al., 1990) in the modern ocean and is considered to be a conservative trace element that is homogeneously distributed even within marginal seas with salinities as low as 14psu (Veizer, 1989; Veizer et al., 1983). The $^{87}Sr/^{86}Sr$-ratio of the continental runoff is more radiogenic than that of seawater, because the latter is buffered by interaction with hydrothermal fluids and the oceanic crust (Richter et al., 1992; Spooner, 1976), with a modern ocean value of

0.709175 (McArthur, 1994). The radiogenic Sr isotope composition of seawater is believed to reflect the dynamics of the Earth`s exogenic system, chiefly its plate tectonics (Veizer, 1988; Veizer et al., 1999). Thus, the changes in $(^{87}Sr/^{86}Sr)_{sw}$ are a function of seafloor spreading, orogenesis, climate, and mountain uplift.

Despite the fact that the $^{87}Sr/^{86}Sr$ system is reasonably well understood, discrepancies between modeled and observed $(^{87}Sr/^{86}Sr)_{sw}$ ratios exist, particularly during the Cenozoic (Vance et al., 2009; Veizer, 1989). Enhancement of weathering rates after deglaciations and tectonic uplifts (Hodell et al., 1989; Krabbenhöft et al., 2010; Porder et al., 2007; Stoll and Schrag, 1998; Taylor and Blum, 1995; Vance et al., 2009) and associated incongruent weathering of silicates (Blum and Erel, 1997), the ease of weathering of island arcs (Allègre et al., 2010), the release of Sr from riverine particulate matter (Jones et al., 2013), and uncertain estimates of the low-temperature alteration of the oceanic crust (Butterfield et al., 2001; Derry, 2009) and groundwater discharge (Basu et al., 2001) all contribute to the divergence of modeling and observations. Furthermore, while the radiogenic Sr isotope system can provide information about the Sr input fluxes to the ocean it is not suitable for quantification of Sr output fluxes. This is due to equal $^{87}Sr/^{86}Sr$ values of seawater and its precipitates, being a consequence of neglected isotope fractionation during mass spectrometric analysis. Modeled Sr concentrations in seawater $([Sr]_{sw})$ therefore have to rely on the less well known $(Sr/Ca)_{sw}$ ratios and seawater calcium concentrations $([Ca]_{sw})$ gleaned from marine carbonates and fluid inclusions, respectively (Horita et al., 2002; Lowenstein et al., 2005; Steuber and Veizer, 2002; Wallmann, 2004).

These limitations can be overcome by extending the Sr isotope systematic to include also the stable Sr isotope ratio $^{88}Sr/^{86}Sr$. The stable Sr isotope variations, expressed as $\delta^{88/86}Sr$ relative to the $SrCO_3$ standard SRM987 distributed by the National Institute of Standards and Technology (NIST) (Fietzke and Eisenhauer, 2006), are calculated using the following relation:

$$\delta^{88/86}Sr\ [‰] = \left(\frac{\frac{^{88}Sr}{^{86}Sr}_{sample}}{\frac{^{88}Sr}{^{86}Sr}_{SRM987}} - 1 \right) * 1000$$

The $^{88}Sr/^{86}Sr$ in modern marine carbonates were found to be distinctly lower than present day seawater (Böhm et al., 2012; Krabbenhöft et al., 2010; Krabbenhöft et

al., 2009). As stated above, changes in $\delta^{88/86}Sr$ signatures of seawater ($\delta^{88/86}Sr_{sw}$) and marine carbonates throughout Earth's history are influenced by both variations in the Sr sources as well as the carbonate output flux. A simultaneous determination of $^{88}Sr/^{86}Sr$- and $^{87}Sr/^{86}Sr$-ratios enables the construction of comprehensive budgets for Phanerozoic oceans, thereby improving our understanding of the interaction between continental weathering, ocean chemistry, and climate change. On glacial/interglacial time scales, Krabbenhöft et al. (2010) pointed out that sea level change with associated changes in weathering regimes leads to changes in $\delta^{88/86}Sr_{sw}$ and intensity of the Sr input flux to the ocean. The goal of this study is to determine the causative mechanisms for variations of $\delta^{88/86}Sr_{sw}$ on Phanerozoic time scales.

2 Materials and methods

The present study includes 177 $\delta^{88/86}Sr$ and $^{87}Sr/^{86}Sr$ measurements from brachiopods, belemnites and carbonate matrices. In addition, in order to establish the Sr isotope fractionation factor between brachiopods and seawater ($\Delta^{88/86}Sr_{cc\text{-}sw}$) we measured 13 modern brachiopod samples from different habitat locations and water temperatures (table A3 in the electronic annex). The $\Delta^{88/86}Sr_{cc\text{-}sw}$ of belemnites was determined by analyzing eleven Jurassic belemnites and brachiopods from the Swabian Alb and Swiss Jura, originating from four stratigraphic units (Table 1) of Middle Oxfordian to Upper Kimmeridgian ages. The samples were embedded in a sponge-microbial marly limestone facies.

The remaining samples are from the Phanerozoic carbonate database published in Veizer et al., (1999). Their assignment to biostratigraphic zones has a resolution of about 1-2Myrs. Note that some of our Permian samples were re-evaluated in a later publication and classified as stratigraphically not well defined due to i) their assignment to Chinese stages or ii) broad geological periods or iii) due to missing lithologic and biostratigraphic information (Korte et al., 2005). Nevertheless, the $^{87}Sr/^{86}Sr$ ratios of our Permian samples are also in accordance with samples that were classified as well preserved and biostratigraphically well defined (Korte et al., 2006; Korte et al., 2005) as is also the case with other samples from the same database of Veizer et al. (1999) and the references therein (see Fig. A3 in the electronic annex). The selected samples are low-Mg calcite shells of brachiopods, belemnites, and some carbonate matrices, mostly originating from 30°S to 30°N paleolatitudes (Veizer et al., 1999). The investigation method and the preservation

state of the samples are discussed in Diener et al. (1996), Veizer et al. (1997a), Veizer et al. (1997b), Azmy et al. (1998), Bruckschen et al. (1999), and Veizer et al. (1999). For this study we selected the best available samples from this database, with low Mg, Mn, and (for belemnites) Fe concentrations and with well clustered $\delta^{18}O$ and $^{87}Sr/^{86}Sr$ ratios for coeval samples from the database; all indicating little diagenetic overprint (Bruhn et al., 1995; Veizer et al., 1999).

Modern low-Mg shells of brachiopods contain less than 460µg/g Mn and 200 to 2150µg/g Sr (Brand et al., 2003; Lepzelter et al., 1983; Morrison and Brand, 1988). Diagenetic alterations usually lead to a decline in Sr and an increase in Mn concentrations (Veizer et al., 1997b). 97% of our fossil brachiopod samples have Sr concentrations in the range of modern species (Table A4 and Fig. A1 in the electronic annex). Sr concentrations >2150µg/g found in early Paleozoic brachiopods are presumably a consequence of naturally higher Sr/Ca ratios of coeval seawater (Steuber and Veizer, 2002). 95% of our fossil brachiopod samples have Mn concentrations less than 460µg/g. Nevertheless, for 30% of our brachiopod samples no Mn and for 25% of our brachiopod samples no Sr concentrations were available. Because of limited brachiopod availability in the Mesozoic, belemnites were used instead as the best available carrier phases (Jones et al., 1994a; Jones et al., 1994b; Smalley et al., 1994; Veizer et al., 1999). Well preserved Phanerozoic fossil belemnite samples have Fe concentrations less than 150µg/g and Mn concentrations less than 20µg/g (Jones et al., 1994a; Jones et al., 1994b). 90% of our samples have Mn concentrations of less than 20µg/g and 71% of our samples have Fe concentrations of less than 150µg/g (Table A4 and Fig. A1 in the electronic annex). For 6% of our belemnite samples no Mn and Fe concentrations were available. Note that there is no correlation between Sr and Mn concentrations for each fossil group in any specific section, indicating a negligible degree of diagenesis in our dataset (Fig. A2 in the electronic annex).

The fossil carbonates originate from Australia, Austria, Belgium, Canada, China, Germany, Hungary, Italy, Latvia, Lithuania, New Zealand, USA, Russia, Slovakia, Sweden, Switzerland, and Ukraine. For further details on stratigraphy, location and age see the electronic annex and references in Veizer et al. (1999).

Sampling procedures and measurement methods followed those of Farkaš et al. (2007a) and Krabbenhöft et al. (2009). To investigate stable Sr isotope fractionation and to correct for mass-dependent Sr isotope fractionation during sample treatment

and mass spectrometric analysis a Sr double spike (DS) method was applied. Depending on Sr concentrations we obtained 0.5 – 10mg carbonate powders from fossil samples by drilling with a conventional dental drill or, alternatively, with a New Wave© micro mill; the latter for higher spatial resolution on thick-sections or for smaller samples. For brachiopods, we sampled the "secondary" (or interior) layer, which is characterized by the highest degree of preservation (Veizer et al., 1997a). For belemnite samples we drilled into one single layer of the rostrum, parallel to its elongation. The modern brachiopods were sampled by mechanically separating a piece of the shell with a pair of teflon tweezers. To remove organic coatings (i.e. periostracum), our modern carbonate samples were reacted in a 10% sodium hypochlorite solution (~1% active chlorine) for at least 12 hours in a teflon PFA vial. The samples were washed in ultrapure water (>18MΩ) afterwards.

All carbonate powders were ultrasonically cleaned twice in ultrapure water for about 30 minutes. All samples were dissolved in 0.5N HNO_3, undissolved residual parts removed, and samples heated in a mixture of 100µl of 30% H_2O_2 and 200µl of 8N HNO_3 at 80°C to dissolve and oxidize organic components. The samples were then split and an $^{87}Sr/^{84}Sr$ DS was added to one split of each dissolved sample. Ion chromatography was performed with BIO-RAD 650µl columns which were filled to one third with Triskem Sr-SPS resin (particle size 50µm to 100µm). In order to verify diagenetic alteration, splits of several samples (Table 1 and table A4 in the electronic annex) were measured also for their $\delta^{13}C$- and $\delta^{18}O$-composition on a Finnigan MAT 252 stable isotope ratio mass spectrometer equipped with a Kiel CARBO device at the mass-spectrometer facilities at GEOMAR. Reproducibility of the in-house carbonate standard (Solnhofen limestone) is 0.05‰ (2 s.d.) for both $\delta^{13}C$ and $\delta^{18}O$. The Ca, Mg, Mn, Fe and Sr concentrations were determined by ICP-MS (Agilent 7500 series) at GEOMAR. The external reproducibility (2 s.d.) on the carbonate standard JCp-1 (Okai et al., 2002) is 2% for Ca, Mg, and Sr and 5% for Mn and Fe concentrations.

Sr isotope analysis was performed using TIMS measurement procedures, which follow the Sr DS-method as outlined by Krabbenhöft et al. (2009). Briefly, the samples were loaded on rhenium ribbon single filaments in combination with a Ta_2O_5-activator. The measurements were carried out on a TRITON TIMS (Thermo-Fisher) at the GEOMAR mass spectrometer facilities. The measurement commenced when signal intensity of 10V on mass 88 was achieved.

The application of the DS-technique in combination with an iterative spike correction algorithm that uses an exponential law for the mass fractionation correction (Krabbenhöft et al., 2009) enables determination of natural $^{88}Sr/^{86}Sr$-ratios in addition to the conventional radiogenic $^{87}Sr/^{86}Sr$-ratios. All conventional radiogenic $^{87}Sr/^{86}Sr$-ratios of the samples were normalized to a $^{86}Sr/^{88}Sr$ ratio of 0.1194 (Nier, 1938). Samples were also corrected for the offset between the measured $^{87}Sr/^{86}Sr$ value of SRM987 of the individual session and the $^{87}Sr/^{86}Sr$-ratio of 0.710240 as published in Veizer et al. (1999).

The external reproducibility (2 s.d.) for all $\delta^{88/86}Sr$ measurements was determined by the repeated analysis of multiple preparations and chromatographic separations of the coral standard JCp-1 (distributed by the Geological Survey of Japan) over a period of 28 months. The resulting $\delta^{88/86}Sr$ value is 0.193±0.022‰ (n=32; 2 s.d.) and is in agreement with previously published data (Krabbenhöft et al., 2010; Krabbenhöft et al., 2009; Ohno and Hirata, 2007). The conventional radiogenic $^{87}Sr/^{86}Sr$-ratio on JCp-1 is 0.709172±0.000022 (n=32; 2 s.d.), also in agreement with previously published data of modern seawater and marine carbonates (e.g. McArthur (1994)). The analytical blank for the entire procedure was determined to be less than 0.3ng Sr, which is <0.1% of the Sr amount in our samples. The radiogenic Sr isotope composition of the blank is 0.7099±0.0006 and therefore not expected to influence the $^{87}Sr/^{86}Sr$ ratio of the samples by more than 3ppm.

3 Results

The $\delta^{88/86}Sr$ values of modern brachiopods range between 0.160‰ and 0.189‰, with a mean of 0.176±0.016‰ (2 s.d., Fig. 1). Accordingly, the $\delta^{88/86}Sr$ of modern brachiopods are identical within the external reproducibility of our method (2 s.d. = 0.022‰).

Among the coeval Jurassic brachiopods and belemnites, two brachiopods have high Fe and Mn concentrations, low $\delta^{18}O$ values, and elevated $^{87}Sr/^{86}Sr$-ratios, all indicating diagenetic alteration (table 1). These samples were excluded from further discussion. The remaining nine samples from three different stratigraphic units have statistically identical $\delta^{88/86}Sr$ values for brachiopods and belemnites in two of three stratigraphic units. In the third stratigraphic unit $\delta^{88/86}Sr$ values for brachiopods are 0.06‰ higher than for belemnites.

We observe significant variations in $\delta^{88/86}Sr$ of Phanerozoic calcium carbonate samples ($\delta^{88/86}Sr_{cc}$, Fig. 2). The mean value of all fossil carbonate samples is 0.16‰. The highest values were found in the late Permian and late Triassic ($\delta^{88/86}Sr_{cc}$ = 0.36‰ and 0.39‰, respectively), and the lowest in the Silurian and middle Permian ($\delta^{88/86}Sr_{cc}$ = 0.07‰ and 0.04‰, respectively). Over the Paleozoic, the data show an overall decrease from the late Ordovician ($\delta^{88/86}Sr_{cc}$ ≈ 0.15‰) to the early Silurian ($\delta^{88/86}Sr$ ≈ 0.10‰) followed by a prolonged rise to 0.25‰ in the early Permian. In the Permian $\delta^{88/86}Sr_{cc}$ decreases to the Phanerozoic minimum of 0.04‰ and increases afterwards up to one of the highest values of the Phanerozoic of 0.36‰ at the P/T transition. In the mid Triassic $\delta^{88/86}Sr_{cc}$ declines back to very low ratios of 0.07‰, followed by an increase in the late Triassic. The late Permian and early Triassic show the highest Phanerozoic rate of change of 0.024‰/Myr. The Jurassic to early Cretaceous belemnite and brachiopod data indicate an increase from ~0.1‰ to ~0.2‰.

4 Discussion

4.1 Sr fractionation factor ($\Delta^{88/86}Sr_{cc\text{-}sw}$) between the carbonate recording phase and seawater

In order to reconstruct the Phanerozoic $\delta^{88/86}Sr_{sw}$ record, the fractionation factor between seawater and the recording carbonate phase needs to be known.
Our results indicate that the $\delta^{88/86}Sr$ values of modern brachiopods are independent of species, habitat location and water temperature with a mean of 0.176±0.016‰ (Fig. 1). We therefore propose that brachiopod samples are a reliable archive for the reconstruction of $\delta^{88/86}Sr$ values of past seawater. This conforms with recent observations from cold water corals (Raddatz et al., 2013) but differs from earlier studies for warm water corals that suggested a temperature-dependent isotope fractionation in carbonates (Fietzke and Eisenhauer, 2006), implying a potential species-dependent biomineralization process analogous to that for Ca isotopes (Farkaš et al., 2007a; Gussone et al., 2005; Nägler et al., 2000).
For the present purposes we assume that the fractionation factor for our species was constant through time. Taking the IAPSO seawater standard as representative for global seawater ($\delta^{88/86}Sr_{IAPSO}$ = 0.386‰ (Krabbenhöft et al., 2009)) we obtain a fractionation factor $\Delta^{88/86}Sr_{cc\text{-}sw}$ of -0.21‰ for modern brachiopods.

Considering the identical, or near identical, $\delta^{88/86}Sr$ values observed in coeval Jurassic brachiopods and belemnites (table 1), we assume, as a first order approach, that their isotope fractionation factors $\Delta^{88/86}Sr_{cc\text{-}sw}$ are identical. In contrast, carbonate matrix samples have significantly higher $\delta^{88/86}Sr$ than the skeletal components and also higher $^{87}Sr/^{86}Sr$ (table 1). This and the variable offset in $\delta^{88/86}Sr$ between macrofossils and their host rocks (carbonate matrix) suggest that the matrix samples are less reliable for the reconstruction of $\delta^{88/86}Sr_{sw}$.

4.2 $\delta^{88/86}Sr$ of Phanerozoic seawater

4.2.1 Sample selection and $\delta^{88/86}Sr_{sw}$ reconstruction

Keeping in mind that Sr represents a trace constituent (i.e. a few hundreds to thousands of µg/g) in the low-Mg calcite of brachiopods and belemnites, one has to seriously consider the possibility that, even in our well preserved Phanerozoic carbonates, the primary marine $\delta^{88/86}Sr$ signature might have been reset or partially modified by diagenetic processes. Based on the models of 'water-rock interactions' (Banner and Hanson, 1990), the degree of diagenetic resetting of Sr isotopes in marine carbonates will be strongly dependent, among other factors, on the concentrations of Sr in the original carbonate and a diagenetic fluid (e.g. pore water). Although a trace constituent, the concentration of Sr in marine biogenic (low-Mg) carbonates is still about two orders of magnitude higher compared to that in pore waters (Richter and DePaolo, 1988). Consequently, relatively large volumes of water have to pass through carbonate rocks in order to significantly alter their Sr isotope composition. The resetting of diagenetically sensitive trace elements, such as Mn and Fe that have distribution coefficients greater than one (Dromgoole and Walter, 1990), does not automatically imply resetting of Sr isotopes (Jones et al., 1994a; Veizer, 1989).

As an analogy to Sr, the amount of sulfate (SO_4^{2-}) in our brachiopod and belemnite shells is also at trace levels (i.e. thousands of µg/g, Kampschulte and Strauss (2004)), and it is also about 1000 times higher than in typical freshwaters (Drever, 1997). Yet, the sulfur isotope ($\delta^{34}S$) data generated from calcite shells yield a systematic and well-defined temporal trend (Kampschulte and Strauss, 2004), in agreement with the independent $\delta^{34}S$ record for Phanerozoic seawater that was reconstructed from marine evaporitic sulfates (Strauss, 1997). Such an excellent agreement between these two recording phases (i.e. 'low-sulfate' carbonates versus

'high-sulfate' evaporites) can only be produced if the low-Mg biogenic carbonates were stabilized at an early diagenetic stage when they were still in contact with the coeval seawater, or seawater-derived pore fluids. This observation give us confidence that the isotope systems of elements, even those that are present in calcitic shells only at trace levels, such as strontium or sulfur, are able to record and preserve (near) primary marine isotope signatures. Nonetheless, and despite the above arguments, we applied also additional criteria for reconstruction of the $\delta^{88/86}Sr_{sw}$ record. Specifically, we used only skeletal carbonates that i) had $^{87}Sr/^{86}Sr$ that differed less than 0.0001 from the measurements on the same samples by Veizer et al. (1999) and ii) also deviated less than 0.0001 from $^{87}Sr/^{86}Sr$ of coeval literature samples that were compiled in Veizer et al. (1999) (see also Table A4 and Fig. A3 in the electronic annex). These selection criteria are believed to be very effective in detecting Sr exchange with surrounding pore waters, as this process would lead to altered $^{87}Sr/^{86}Sr$ ratios. Given their tendency for diagenetic exchange, we did not utilize the carbonate matrix samples for interpretation purposes in the present study. This selection procedure resulted in 153 samples for the $\delta^{88/86}Sr_{sw}$ record.

Applying the fractionation factor of $\Delta^{88/86}Sr_{cc\text{-}sw}$ = -0.21‰ to our carbonate recording phases (brachiopods and belemnites), the Phanerozoic $\delta^{88/86}Sr_{sw}$ can be reconstructed (Fig. 3). The data points in the Late Triassic at 202Ma and in the Late Jurassic at 158Ma were linearly interpolated and here indicated by a dashed line. Limitations due to the accuracy of the age model, analytical precision, and preservation state of the samples lead to the fact that the derived $\delta^{88/86}Sr_{sw}$ and $(^{87}Sr/^{86}Sr)_{sw}$ trends are bands rather than curves (Veizer et al., 1997b). The width of this $\delta^{88/86}Sr_{sw}$ band is difficult to determine due to the comparatively small number of available data points but indications from 13 modern brachiopods (2 s.d. = 0.016‰) and eight coeval Ordovician samples (2 s.d. = 0.031‰) suggest that it is in the range of 0.06‰.

4.2.2 Interpretation of the $\delta^{88/86}Sr_{sw}$ record

The Phanerozoic $\delta^{88/86}Sr_{sw}$ curve is calculated with a 5 Myr running mean, based on 153 measurements. $\delta^{88/86}Sr_{sw}$ range between 0.25‰ and 0.60‰, and has a mean value of 0.37 ± 0.12‰ (2 s.d.). Phanerozoic $\delta^{88/86}Sr_{sw}$, like $\delta^{44/40}Ca_{sw}$, were always isotopically heavier than the mantle sources ($\delta^{88/86}Sr_{hyd\text{-}in}$ = 0.27‰ (Charlier et al., 2012; Krabbenhöft et al., 2010); $\delta^{44/40}Ca_{hyd\text{-}in}$ = 1.1‰ (Huang et al., 2010)), the latter

defining the lower boundary conditions for isotope trends (Fig. 3). Comparison of Phanerozoic $(^{87}Sr/^{86}Sr)_{sw}$ and $\delta^{88/86}Sr_{sw}$ records (Fig. 3) shows that they are not correlated ($r^2 = 0.003$; $p = 0.35$, see Fig. A4 in the electronic annex for details). The $^{87}Sr/^{86}Sr$ has characteristic ~60Myrs oscillations superimposed on a general decline across the Paleozoic (Prokoph et al., 2008). In contrast, $\delta^{88/86}Sr_{sw}$ is decreasing from the Ordovician (~0.35‰) to the Silurian (~0.30‰) but rises to ~0.50‰ in the Early Permian. During the P/T transition, both isotope systems show similar patterns with their Paleozoic minimum values ($\delta^{88/86}Sr_{sw} \approx 0.25$‰, $(^{87}Sr/^{86}Sr)_{sw} \approx 0.7070$) in the Late Permian at ~260Ma and a steep increase until the early Triassic at ~245Ma ($\delta^{88/86}Sr_{sw} \approx 0.54$‰, $(^{87}Sr/^{86}Sr)_{sw} \approx 0.7082$). However, the rate of change is significantly faster for $^{88}Sr/^{86}Sr$ (~0.000162/Myr) than for $^{87}Sr/^{86}Sr$ (0.000080/Myr) (see also Fig. 9). Note that these systems could not have been linked via mass-dependent isotope fractionation, because the latter is neglected during the mass spectrometric analysis for $^{87}Sr/^{86}Sr$. From the Late Triassic to Late Jurassic the radiogenic Sr again declines to ~0.7069 followed by a rise to ~0.7075 during the Early Cretaceous (McArthur et al., 2001). In contrast, $\delta^{88/86}Sr_{sw}$ declines abruptly in the mid-Triassic to ~0.28‰ and then rises to ~0.48‰ in the Late Triassic. The sparse data for the Late Jurassic and Early Cretaceous indicate a slight increase from ~0.29‰ to ~0.40‰. In summary, the $\delta^{88/86}Sr_{sw}$ and $(^{87}Sr/^{86}Sr)_{sw}$ generally differ both, on short and long term time scales, as well as in the rates of changes, despite some similarities in the Permian and at the Jurassic/Cretaceous boundary. These ratios must be therefore controlled by different mechanisms on Phanerozoic time scales. The $\delta^{88/86}Sr_{sw}$ variations reflect changes in the carbonate related flux of Sr (net flux which is associated with carbonate burial and dissolution; $F(Sr)_{carb}$), hydrothermally introduced fluids and precipitation ($F(Sr)_{hyd\text{-}in}$, $F(Sr)_{alt}$), silicate and carbonate continental weathering ($F(Sr)_{ws}$, $F(Sr)_{wc}$), and their isotope signatures ($\Delta^{88/86}Sr_{carb\text{-}sw}$, $\delta^{88/86}Sr_{hyd\text{-}in}$, $\Delta^{88/86}Sr_{alt\text{-}sw}$, $\delta^{88/86}Sr_{ws}$, $\delta^{88/86}Sr_{wc}$) (Krabbenhöft et al., 2010). Due to similar $\delta^{88/86}Sr$ values for the silicate weathering and hydrothermal input fluxes (~0.27‰; Table 2), variations in the ratio of these fluxes have a negligible effect on $\delta^{88/86}Sr_{sw}$. In addition, the hydrothermal $\delta^{88/86}Sr_{hyd\text{-}in}$ signatures are not variable over time as the Earth`s mantle is supposed to represent a homogenized reservoir with respect to stable Sr isotopes. The fractionation factor for inorganic calcite precipitates in the oceanic crust ($\Delta^{88/86}Sr_{alt\text{-}sw} = -0.01$‰ (Böhm et al., 2012)) is also considered to be constant through time. In contrast, changes in $F(Sr)_{wc}$, $F(Sr)_{carb}$ and the related

isotope fractionation factor $\Delta^{88/86}Sr_{carb\text{-}sw}$, as well as imbalances between Sr input and output fluxes may have a large impact on $\delta^{88/86}Sr_{sw}$ (Krabbenhöft et al., 2010). In particular, the carbonate output flux $F(Sr)_{carb}$ is an important determinant of $\delta^{88/86}Sr_{sw}$, while for radiogenic Sr isotopes it is the ratio of the input fluxes ($F(Sr)_{ws}$, $F(Sr)_{wc}$, and $F(Sr)_{hyd\text{-}in}$) that is of importance.

This behavior of Phanerozoic $\delta^{88/86}Sr_{sw}$ has similarities with the Ca isotope systematics ($\delta^{44/40}Ca_{sw}$, Fig. 3) which is also controlled mostly by carbonates as the main output flux (Blättler et al., 2012; Farkaš et al., 2007a). Accordingly, we expect similar trends in $\delta^{88/86}Sr_{sw}$ and $\delta^{44/40}Ca_{sw}$. Both isotope systematics appear to reflect the scenarios of “aragonite” and “calcite” seas (Stanley and Hardie, 1998). In details, however, the mechanisms differ. The $\delta^{88/86}Sr_{sw}$ reflects the fact that the Sr content in seawater precipitates (aragonite vs. calcite) differ by a factor of 3-10 (Milliman et al., 1974; Steuber and Veizer, 2002) while for calcium isotopes the isotopic fractionation factors are different (Blättler et al., 2012; Farkaš et al., 2007a) for these two carbonate polymorphs. Specifically, the higher Ca isotope fractionation factor of aragonite in contrast to calcite results in higher $\delta^{44/40}Ca_{sw}$ during “aragonite” seas (Blättler et al., 2012; Farkaš et al., 2007a; Farkaš et al., 2007b). As a result, both isotopic systems are positively correlated over the Phanerozoic ($\delta^{44/40}Ca_{sw} = 3.72 * \delta^{88/86}Sr_{sw}$; $r^2 = 0.094$; $p = 3*10^{-8}$), particularly during the Paleozoic ($\delta^{44/40}Ca_{sw} = 4.03 * \delta^{88/86}Sr_{sw}$; $r^2 = 0.264$; $p = 1*10^{-17}$). Less correlated isotope trends in the Mesozoic are probably related to the shift to more sophisticated calcitic biomineralizers with a $\Delta^{44/40}Ca_{cc\text{-}sw}$ that is more similar to that of aragonite (Blättler et al., 2012). Interestingly, autocorrelation results indicate that the Paleozoic $\delta^{44/40}Ca_{sw}$ trend lags ~13Myrs behind $\delta^{88/86}Sr_{sw}$. From the geochemical point of view we cannot yet explain this phase shift as both elements have similar marine cycles and residence times (Hodell et al., 1990; Zhu and Macdougall, 1998). Despite the similarity between $\delta^{88/86}Sr_{sw}$ and $\delta^{44/40}Ca_{sw}$ on the long-term, the isotope trends often diverge on shorter time scales. Due to the complexity of the system it is difficult to assign these discrepancies to specific causes. Additional processes, not as yet well constrained, such low temperature alteration of the oceanic crust, local element cycling effects, and/or dolomitization may play a role. For example, Ca isotopes in primary dolomites were found to be lighter than in the initial fluid, leaving the remaining fluid isotopically heavier (Krause et al., 2012). Theoretically (Artemov et al., 1967), elements released during the process of dolomitization should be isotopically light. For Ca, this is

supported by one study (Farkaš et al., 2013), but negated by another (Holmden, 2009). The low temperature alteration of island arcs and oceanic islands has not been studied for Ca and stable Sr isotopes. We assume that this process is a source of relatively light Sr compared to seawater due to low $\delta^{88/86}Sr$ of mid ocean ridge (MOR) fluids (Krabbenhöft et al., 2010) and basalts (Charlier et al., 2012; Moynier et al., 2010; Ohno and Hirata, 2007; Souza et al., 2010). Further, some of the scatter in the long term $\delta^{44/40}Ca_{sw}$ and $\delta^{88/86}Sr_{sw}$ trends could be related to the effect of local Ca and Sr cycling in epeiric settings (Holmden et al., 2012).

In summary, the long term trends of $\delta^{88/86}Sr_{sw}$ and $\delta^{44/40}Ca_{sw}$ resemble each other but differ from $(^{87}Sr/^{86}Sr)_{sw}$. The above coherence is best explained by similar marine global budgets due to the importance of carbonate fluxes and associated isotope fractionations for the cycles of both elements. This coherence breaks down on shorter time scales, perhaps due to the impact of as yet not well defined factors, such as carbonate mineralogy, dolomite formation, local element cycling effects, changes in biogenic and inorganic carbonate precipitation, and/or diagenetic post-depositional transformation of aragonite to calcite which might have a different influence on $\delta^{88/86}Sr_{sw}$ and $\delta^{44/40}Ca_{sw}$ (Blättler et al., 2012; Farkaš et al., 2007a; Holmden et al., 2012).

4.3 Numerical box model of the oceanic C, Mg, Ca, and Sr budget

To quantify our qualitative observation we extended the numerical box models from Farkaš et al. (2007a) and Wallmann (2004), which represent a global budget with coupled carbon, magnesium, calcium, and strontium, by adding a Sr flux for hydrothermal alteration ($F(Sr)_{alt}$) and an isotope mass balance equation for seawater $\delta^{88/86}Sr$ (see Fig. 4 for model scheme and electronic annex for mass balance equations). This enables the calculation of the Phanerozoic Sr budget without using the $(Sr/Ca)_{sw}$ ratios (Wallmann, 2004) with its relatively large uncertainties (Steuber and Veizer, 2002), except for the last 125Myr where the model has to be forced by this variable due to the absence of $\delta^{88/86}Sr$ data. The respective isotope compositions of the Sr fluxes are summarized in table 2. With the three (isotope) mass balance equations for $[Sr]_{sw}$, $(^{87}Sr/^{86}Sr)_{sw}$, and $\delta^{88/86}Sr_{sw}$ and independent estimates for silicate and carbonate continental weathering rates ($F(Sr)_{ws}$ and $F(Sr)_{wc}$, see Wallmann (2004) for details) it is possible to calculate changes in all Sr fluxes, including the carbonate related net flux $F(Sr)_{carb}$. The mean temporal resolution of our dataset is ~1 sample per 3Myrs which is high enough for identifying perturbations in

the marine Sr cycle that act on timescales >5Myrs. Processes with shorter durations are not expected to produce significant changes in seawater Sr isotopes (Veizer, 1989).

In our model simulation the $\Delta^{88/86}Sr_{carb\text{-}sw}$ is kept constant at -0.24‰, in the range of that for modern carbonates (-0.12‰ to -0.37‰ (Eisenhauer et al., 2011; Krabbenhöft et al., 2010)). Therefore, $\delta^{88/86}Sr_{sw}$ depends only on changes in $F(Sr)_{carb}$. In contrast, Blättler et al. (2012) and Farkaš et al. (2007) suggested that the Paleozoic and Early Mesozoic $\delta^{44/40}Ca_{sw}$ trend is mainly dependent on changes in the fractionation factor between calcite and aragonite. To test if this also holds true for stable Sr isotopes, we applied a sensitivity study to test the impact of $\Delta^{88/86}Sr_{carb\text{-}sw}$ on $\delta^{88/86}Sr_{sw}$, showing that the latter cannot be explained solely by the changing fractionation factor between carbonates and seawater, as modeled $\Delta^{88/86}Sr_{carb\text{-}sw}$ (0.7‰ to -1.3‰) considerably exceed the modern $\Delta^{88/86}Sr_{cc\text{-}sw}$ range of -0.12‰ to -0.37‰ (see the electronic annex; (Eisenhauer et al., 2011; Krabbenhöft et al., 2010)).

4.3.1 Results for Sr fluxes and seawater Sr concentration

The changes in Phanerozoic $[Sr]_{sw}$ and Sr fluxes, based on our numerical model simulation are summarized in Fig. 5. $[Sr]_{sw}$ varies from 24 and 300µmol/l and has a mean of 151µmol/l. The highest concentrations were calculated for the Ordovician to the Devonian and the Cretaceous and the lowest for the Permian and the Triassic. The carbonate related net Sr flux is also variable, ranging from an output of $-4.7x10^{10}$mol/yr to an input of $2.3x10^{10}$mol/yr with a mean of $-1.6x10^{10}$mol/yr (Fig. 5). The Permian/Triassic boundary is associated with a highly negative mean $F(Sr)_{carb}$ of $-3.4x10^{10}$mol/yr during a 15Myrs time interval between ~260Ma and ~245Ma. This flux and $F(Sr)_{ws}$ appear to be the most important variables controlling the Phanerozoic oceanic Sr budget. In general, the mean $F(Sr)_{carb}$ appears to be slightly weaker during the Paleozoic ($-1.3x10^{10}$mol/Myr) than during the Mesozoic ($-2.0x10^{10}$mol/Myr), presumably a consequence of additional carbonate burial in the pelagic zone, that commenced in the Mesozoic with the appearance of major planktic calcifiers (Wallmann, 2001).

The modeled modern $F(Sr)_{carb}$, $F(Sr)_{ws}$, and $F(Sr)_{wc}$ are significantly lower than published estimates for modern Sr fluxes ($-17.4x10^{10}$mol/yr and ~$5x10^{10}$mol/yr for carbonate burial and combined silicate and carbonate continental weathering fluxes, respectively (Basu et al., 2001; Krabbenhöft et al., 2010; Palmer and Edmond, 1989)). Vance et al. (2009) suggested that observations for modern element fluxes to

the ocean, while broadly accurate, are not representative for elements that have a longer residence times than the duration of Quaternary glacial/interglacial cycles (see also Stoll and Schrag (1998)). In particular, post-glacial weathering could be as much as ~10 times faster due to the demise of continental ice sheets leaving behind a fertile, finely ground substrate (Porder et al., 2007; Taylor and Blum, 1995; Vance et al., 2009; White and Brantley, 2003). The modeled Sr weathering and burial rates appear to confirm that the modern short term fluxes exceed their long term averages gained from the long term integrated isotope records. In particular, according to our model results, short term Sr carbonate burial fluxes are significantly higher in the modern ocean, when compared to average Quaternary values, implying a nearly instantaneous reaction of the modern carbonate system to increased Sr input fluxes from the continents.

4.3.2 Calcite and aragonite seas

With an independent modeled estimate for $[Sr]_{sw}$, both the $(Sr/Ca)_{sw}$ ratio and how it relates to Sr and Ca carbonate output fluxes, here defined as $D(F)_{Sr}$, can be reconstructed by our model.

$$D(F)_{Sr} = \left| \frac{\left(F(Sr)_{carb} \Big/ F(Ca)_{carb} \right)}{(Sr/Ca)_{sw}} = \frac{(Sr/Ca)_{carb}}{(Sr/Ca)_{sw}} \right|$$

The coefficient $D(F)_{Sr}$ is representative for the global average Sr/Ca partitioning coefficient in marine carbonates D_{Sr} which is about 0.1 and 1.0 for the calcite and the aragonite end members, respectively (Milliman et al., 1974). The $F(Ca)_{carb}$ in our model is forced by carbonate saturation, as discussed in Wallmann (2004). These results agree well with the $(Sr/Ca)_{sw}$ curve reconstructed from Phanerozoic carbonates (Steuber and Veizer, 2002; Fig. 6).

Long term modeled trends for $[Sr]_{sw}$, $(Sr/Ca)_{sw}$, and $D(F)_{Sr}$ mimic the proposed "calcite" and "aragonite" seas scenario (Stanley and Hardie, 1998) (Fig. 5 and Fig. 6). In particular, high $(Sr/Ca)_{sw}$, high $[Sr]_{sw}$, and low $D(F)_{Sr}$ are associated with "calcite seas" whereas low $(Sr/Ca)_{sw}$, low $[Sr]_{sw}$, and high $D(F)_{Sr}$ are associated with "aragonite seas". This is a consequence of about 3-10 times higher mean Sr concentrations in aragonite than in calcite (Milliman et al., 1974; Steuber and Veizer, 2002). Our $D(F)_{Sr}$ ranging between 0.08 and 1.23 (mean of 0.21) falls within values reported for calcite/aragonite end members. We observe a higher mean $D(F)_{Sr}$ of

0.52 during “Aragonite II” and a lower mean $D(F)_{Sr}$ of 0.13 during “Calcite I and II” (Fig. 6), with superimposed high order oscillations, particularly during “Aragonite II”. Our model results support the proposition that secular changes in the dominant mineralogy of non-skeletal carbonate precipitates (Sandberg, 1983; Stanley and Hardie, 1998) have a large influence on $F(Sr)_{carb}$, $D(F)_{Sr}$, and $(Sr/Ca)_{sw}$. The dominant carbonate mineralogy is expected to be controlled by $(Mg/Ca)_{sw}$, because calcite forms only below a critical $(Mg/Ca)_{sw}$ ratio, which is ~5/1 at 6°C (Morse et al., 1997). The causative mechanisms for changing $(Mg/Ca)_{sw}$, involving seafloor spreading, dolomitization and associated changes in sea level are still being debated (Veizer and Mackenzie, 2010). Theoretically, low spreading rates during “aragonite seas” should lead to high $(Mg/Ca)_{sw}$ ratios and low sea levels (Hardie, 1996), inhibiting the precipitation of inorganic calcite and leading to relatively low $(Sr/Ca)_{sw}$, high $D(F)_{Sr}$ and high $\delta^{88/86}Sr_{sw}$ as a consequence of a large Sr output flux of isotopically light Sr. This scenario is similar to that advocated for Ca isotopes (Farkaš et al., 2007a), except that the $\delta^{44/40}Ca_{sw}$ were interpreted to reflect changes in Ca isotope fractionation factors between calcite and aragonite (Blättler et al., 2012; Farkaš et al., 2007a).

4.3.3 The effect of changing sea level and ocean anoxia on the marine carbonate budget

Carbonate burial and dissolution are believed to have been closely linked to changes in seawater chemistry induced by ocean anoxia and acidification (Knoll et al., 1996; Payne et al., 2010; Riebesell et al., 1993; Woods et al., 1999). Massive weathering and recrystallization of continental carbonate shelves during sea level low stands could also contribute an additional flux of Sr to the ocean (Krabbenhöft et al., 2010; Stoll and Schrag, 1998). Separately, or in combination, this could lead to a rise in $F(Sr)_{carb}$.

4.3.3.1 The effect of changing sea levels on the marine carbonate budget

The Phanerozoic $F(Sr)_{carb}$ values are generally negative, implying a net output flux of Sr by carbonate burial, but turns positive during six time intervals suggesting that carbonate dissolution exceeds carbonate burial of Sr (Fig. 7). Potentially, carbonate dissolution may arise from ocean acidification or weathering and recrystallization of carbonate shelves during sea level low stands. Five of the six positive events occur during glacial intervals and thus sea level low stands, consistent with the scenario of

weathering/recrystallization of carbonate shelves. Further, coeval atmospheric pCO_2 concentrations are considered to be lower during glacial periods which impede the acidification induced dissolution of carbonates scenario. In the remaining case in the Early Triassic (~238Ma) no glaciations were documented in the geological record implicating acidification as a causative factor.

4.3.3.2 The effect of ocean anoxia on the Permian/Triassic and remaining Phanerozoic marine carbonate budget

The three intervals at about 313Ma, 246Ma, and 93Ma with highly negative $F(Sr)_{carb}$ (<-4x10^{10}mol/yr) require massive burial of carbonates (Fig. 7). The most prominent excursion in $F(Sr)_{carb}$, which is based on ten brachiopod samples from six different sections (Fig. 2 and table A4 in the electronic annex), is observed at the Permian/Triassic (P/T) boundary.

The $\delta^{88/86}Sr_{sw}$ trend from the Late Permian to the Early Triassic period (~260Ma to ~245Ma) reflects a prolonged period of enhanced carbonate burial, on average -3.4x10^{10}mol Sr/yr, with a maximum immediately prior to the P/T boundary, coinciding with declining $[Sr]_{sw}$ (Fig. 8). The diminished Sr (and also Ca) inventories and ocean residence times, as well as the lack of the deep-sea $CaCO_3$ compensation in the Neritan Ocean (Zeebe and Westbroek, 2003) increased the sensitivity of the Sr and Ca isotope systems to changes in their input/output fluxes. This may be the reason for the relatively large and rapid variations observed in the $\delta^{88/86}Sr_{sw}$, $(^{87}Sr/^{86}Sr)_{sw}$, and $\delta^{44/40}Ca_{sw}$ records across the P/T boundary (Payne and Clapham, 2012). Note, that these exceptionally high carbonate burial rates modeled for the P/T interval lasting about 15Myrs require an additional alkalinity flux, such as extensive Bacterial Sulfate Reduction (BSR), a process that produces large amounts of bicarbonate (HCO_3^-) while not contributing extra Sr and Ca to the ocean (see electronic annex for other potential alkalinity input fluxes). This BSR-controlled HCO_3^- production in deeper waters was proposed earlier by the ocean overturn theory (Knoll et al., 1996). This hypothesis implies widespread and long-lasting anoxic bottom water conditions during the Late Permian and Early Triassic times. Note that the timing of the P/T mass extinction and anoxia is heavily discussed in the literature, ranging from an instantaneous event to an event lasting for ~10Myrs (Wignall, 2007). Our model results are also in general accord with the geological record that shows a contemporaneous long term rise in $\delta^{34}S$ of carbonate associated sulfates (CAS) values with distinct short term maxima at the P/T boundary (Gorjan and Kaiho, 2007;

Kaiho et al., 2006; Kampschulte and Strauss, 2004; Luo et al., 2010; Newton et al., 2004; Payne and Clapham, 2012) and the suppression of deep-sea chert deposition ascribed to lethal superanoxic conditions that decreased radiolarian productivity in pelagic water (Isozaki, 1997) (Fig. 8). The suggested low seawater sulfate concentrations of about 1 to 4 mmol/l (Luo et al., 2010), relatively high $\delta^{34}S_{CAS}$ signatures of more than 30 ‰ (Kampschulte and Strauss, 2004), the occurrence of pyrite in P/T sediments (Wignall and Twitchett, 2002) as a consequence of high BSR rates, and short term distribution patterns of redox-sensitive U ($\delta^{238}U$) and Mo isotopes in coeval sediments (Brennecka et al., 2011; Zhou et al., 2009) are also consistent with such a scenario.

Accordingly, we argue that the massive carbonate formation suggested by our $\delta^{88/86}Sr_{sw}$ record and related model results was sustained and possibly triggered by BSR, producing large amounts of alkalinity in anoxic waters and sediments. This hypothesis could also explain the inorganic precipitation of sea-floor $CaCO_3$ cements that are observed in Late Permian reef complexes and Early Triassic carbonate platforms and pelagic plateaus (Grotzinger and Knoll, 1995; Kershaw et al., 2011; Knoll et al., 1996; Riding and Liang, 2005; Woods et al., 1999). The long lasting anoxic conditions may have been supported and amplified by a combination of additional factors, such as global warming (Wignall and Twitchett, 2002), a stagnant and stratified ocean (Knoll et al., 1996), and long term high nutrient fluxes to the oceans from the weathering of coal-swamp deposits (Fig. 8; Berner and Canfield, 1989). In particular, an enhanced influx of nutrients may have increased marine export production causing a significant transfer of atmospheric CO_2 to the deep ocean, enhanced BSR and alkalinity generation in anoxic waters and sediments and extensive carbonate and pyrite burial at the seafloor.

We argue that the intermittent overturning of anoxic deep seawater bringing CO_2- and H_2S-rich toxic waters to the surface ocean considerably affected the marine biodiversity during the end-Permian extinctions, as documented at the P/T boundary extinction horizons in South China, where short-term decreases in $\delta^{34}S_{CAS}$ and $\delta^{238}U$ are interpreted by a release of isotopically light H_2S from intermediate waters to the surface (Brennecka et al., 2011; Payne and Clapham, 2012). The high $\delta^{34}S_{CAS}$ in the Anisian stage (Fig. 8) suggest that such deep-sea anoxic conditions were still present ~10Myrs after the P/T event (Isozaki, 1997; Kampschulte and Strauss, 2004; Newton et al., 2004). This could explain the prolonged biotic recovery and diversification of

marine life after the end-Permian mass extinctions (Chen and Benton, 2012; Knoll et al., 1996; Wignall and Twitchett, 2002).

The overall long-term harsh conditions for marine life appear to be punctuated by a short-term ocean acidification event as seen from petrological studies and the $\delta^{44/40}Ca_{sw}$ record amplifying and accelerating mass extinctions as seen at the P/T boundary (Payne and Clapham, 2012; Sobolev et al., 2011). This short term acidification event is not visible in our long-term $\delta^{88/86}Sr_{sw}$ record, but we anticipate that a negative excursion in $\delta^{88/86}Sr_{sw}$, similar to that observed for Ca isotopes (Hinojosa et al., 2012; Payne et al., 2010), might be observed in future high resolution studies across the P/T boundary. Therefore, the predicted long term seawater anoxia is not necessarily in contradiction to the occurrence of a short term ocean acidification event on the order of a few hundred thousand years (Payne and Clapham, 2012; Sobolev et al., 2011). Probably, the combination of both short term and long term processes is necessary to explain the magnitude of the P/T mass extinction. In particular, the combination of long term seawater anoxia and short term ocean acidification as observed by previous studies may then explain why the Siberian Traps were much more damaging to biota than other Large Igneous Provinces (LIPs) of comparable size.

Two other time intervals, in the Carboniferous and Cretaceous, also have highly negative $F(Sr)_{carb}$. For the Carboniferous, there is no evidence for seawater anoxia at about 320Ma. The record has to be therefore interpreted as resulting from either i) intense carbonate burial by biogenic and inorganic $CaCO_3$ precipitation or from ii) ocean anoxia and the related buildup of alkalinity for which no evidence as yet exists in the geological record. For the Cretaceous, several ocean anoxic events (OAE) are recorded in marine sediments (Jenkyns, 2010) and we therefore suggest that the modeled massive carbonate burial rates at the Cenomanian/Turonian boundary (~94Ma) may be linked to changes in seawater carbonate chemistry during OAE2 similar to the P/T period (Knoll et al., 1996). In summary, we modeled several emerging maxima and minima in Phanerozoic $F(Sr)_{carb}$ values of which the majority could be related to time intervals of glaciations or ocean anoxia. Therefore, we propose that the marine carbonate budget is closely related to the occurrence of these phenomena.

4.3.4 Changes in Sr residence time

The Phanerozoic Sr residence time (τ_{Sr}) was calculated from steady state Sr input and output fluxes (Fig. 9). As this assumption is not valid (Fig. 5), the true τ_{Sr} falls between these two estimates bracketed by the grey band in figure 9. This band has the broadest width during times of large imbalances between Sr input and output fluxes and the smallest width at times of equal Sr fluxes. Calculated τ_{Sr} varies between ~1Myrs for the P/T ocean and ~20Myrs for the Silurian, with a long term mean of ~9Myrs (modern value ~2.5Myrs, Hodell et al., 1990) implying a twenty-fold change in the sensitivity of the Sr isotope systems to external perturbations caused by flux imbalances (Fig. 9). Here, sensitivity is defined as the susceptibility to large rates of changes in seawater isotope ratios. Since the system will be particularly sensitive during periods with short residence times it is not surprising that the highest rates of change for both $(^{87}Sr/^{86}Sr)_{sw}$ and $(^{88}Sr/^{86}Sr)_{sw}$ are observed in the P/T ocean. High rates of change ($d(^{88}Sr/^{86}Sr)_{sw}/dt$) are also observed during the Carboniferous and Late Ordovician period, while high $d(^{87}Sr/^{86}Sr)_{sw}/dt$ are observed during mid-Permian and mid-Ordovician (Fig. 9). The rates of change of the two isotope systems are not always correlated and therefore they are likely controlled by different parameters. The mean rate of change for $^{88}Sr/^{86}Sr$ ($0.000061 Myr^{-1}$) is more than two times higher compared to $^{87}Sr/^{86}Sr$ ($0.000027 Myr^{-1}$). The former is mostly a response to carbonate burial and Sr flux imbalances while the latter is controlled by the balance between continental weathering and hydrothermal activity. Note that the $\delta^{88/86}Sr_{sw}$ data distribution is considerably sparser when compared to the high resolution $(^{87}Sr/^{86}Sr)_{sw}$ curve, which leads to lower calculated rates of change. Ultimately, our results show that ocean residence times should be considered as variable through time which has consequences for the sensitivity of element and isotope systems to perturbation.

5 Conclusions

This study investigates changes of $\delta^{88/86}Sr$ in Phanerozoic seawater reconstructed from marine fossil brachiopods and belemnites. The $\delta^{88/86}Sr$ for modern brachiopods appears to be independent of species, water temperature, and habitat location, with the mean of 0.176‰, corresponding to a fractionation factor between skeletal carbonate and seawater of $\Delta^{88/86}Sr_{cc\text{-}sw}$ of -0.21‰. In contrast to brachiopods and belemnites which appear relatively robust to diagenetic exchange, carbonate matrix

samples are strongly affected by diagenetic processes, restricting their use as a carbonate recording phase for stable strontium isotopes of seawater. Data points assessed as reliable show major fluctuations in $\delta^{88/86}Sr_{sw}$, suggesting large imbalances in the Sr budget of the Phanerozoic ocean which were mainly caused by carbonate burial and dissolution. $F(Sr)_{carb}$ ranged between $-4.7x10^{10}$mol/yr and $+2.3x10^{10}$mol/yr, resulting in $[Sr]_{sw}$ from 24µmol/l to 300µmol/l. On short term time scales, changes in $\delta^{88/86}Sr_{sw}$ and $[Sr]_{sw}$ are related to carbonate burial, carbonate shelf recrystallization/weathering, carbonate dissolution and to ocean anoxia. In particular, the $\delta^{88/86}Sr_{sw}$ record and related model results suggest enhanced carbonate burial from ~260Ma to ~245Ma in the P/T ocean that are potentially related to carbonate alkalinity production via BSR in deep anoxic waters and sediments in a stratified ocean. On long term time scales, changes in modeled $\delta^{88/86}Sr_{sw}$, $(Sr/Ca)_{sw}$, and $D(F)_{Sr}$ correspond to times of the proposed “aragonite” and “calcite” seas (Stanley and Hardie, 1998; Steuber and Veizer, 2002). The carbonate related Sr flux of the ocean appears to have been the main controlling factor on $\delta^{88/86}Sr_{sw}$. This differs from the $^{87}Sr/^{86}Sr$ systematics that reflects mostly the balance between continental weathering and hydrothermal activity. Our model results suggest that the Sr residence time varies throughout the Phanerozoic and ranges between about 1Myrs and 20Myrs, with the highest rate of change for both $\delta^{88/86}Sr_{sw}$ and $(^{87}Sr/^{86}Sr)_{sw}$ during the times of low τ_{Sr}.

6 Tables and figures

6.1 Tables

Table 1 – The radiogenic and stable Sr isotope composition and element concentrations of Jurassic brachiopods, belemnites, and their host limestones (matrices). Samples are from four different sections in the Swabian Alb and Swiss Jura.

Running No.	*Archive*	*Species*	*Age [Ma]*	*Ca [wt%]*	*Mg [wt%]*	*Fe [µg/g]*	*Mn [µg/g]*	*Sr [µg/g]*	*$\delta^{18}O$ [‰]*	*$\delta^{13}C$ [‰]*	*$^{87}Sr/^{86}Sr$*	*$\delta^{88/86}Sr$ [‰]*
Swabian Alb, Ursental section (Bed 2-9), Upper Kimmeridgian, Aulacostephanus mutabilis zone												
Ur2-9-68	Brachiopod	Lacunosella multiplicata	152.8	39.85	0.11	149	13	455	-1.29	2.79	0.707035	0.149
	Matrix		152.8								0.707911	0.250
Ur2-9-70 bra[a]	Brachiopod	Lacunosella multiplicata	152.8	39.57	0.39	2845	72	439	-3.25	1.35	0.707439	0.129
Ur2-9bel	Belemnite	Belemnite indet.	152.8	39.68	0.27	371	26	506			0.706994	0.144
Swabian Alb, Geisingen section (Bed 13), Lower Kimmeridgian, Crussoliceras divisum zone												
Gei13	Belemnite	Belemnite indet.	153.3	39.60	0.28	55	3	1200			0.707007	0.133
	Matrix 1/2		153.3								0.707876	0.355
	Matrix 2/2		153.3								0.707400	0.152
Gei13	Brachiopod	Nucleata nucleata	153.3	39.67	0.28	469	33	530	-2.22	2.28	0.707017	0.141
Swabian Alb, Gosheim section (Bed 7), Upper Oxfordian, Epipeltoceras bimammatum zone												
Gos7-54	Brachiopod	Lacunosella subsimilis	156.1	39.86	0.10	167	23	365			0.706998	0.189
Gos7-007-87	Brachiopod	Placothyris rollieri	156.1	39.68	0.27	670	21	506	-0.86	2.80	0.707091	0.144
Gos7	Belemnite	Belemnite indet.	156.1	39.52	0.35	94	9	1237			0.706983	0.109
Swiss Jura, Holderbank section (Bed 23), Middle Oxfordian, Gregoryceras transversarium zone												
Hol23[a]	Brachiopod	Argovithyris birmensdorfensis	157.9	39.53	0.42	4808	340	522	-5.40	0.64	0.708413	0.204
Hol23	Belemnite	Belemnite indet.	157.9								0.706832	0.071
Hol23	Belemnite	Belemnite indet.	157.9								0.706885	0.079
	Matrix		157.9								0.707602	0.297

[a] Samples show increased Fe and Mn concentrations, low coeval $\delta^{18}O$ values compared to Veizer et al. (1999), and high coeval $^{87}Sr/^{86}Sr$-ratios compared to McArthur et al. (2001) (Look-Up Table Version 4: 08/ 04), both indicating diagenetic alteration of these samples.

Table 2 – Definition and isotope composition of Sr fluxes considered in the numerical model

Strontium flux	*Abbrev.*	*$\delta^{88/86}Sr$*	*$^{87}Sr/^{86}Sr$*
Silicate continental weathering input flux	$F(Sr)_{ws}$	$\delta^{88/86}Sr_{ws}$ = 0.27‰ [a]	$^{87}Sr/^{86}Sr_{ws}$ = variable [b]
Carbonate continental weathering input flux	$F(Sr)_{wc}$	Mean $\delta^{88/86}Sr_{carb}$ of preceding 200 Ma	Mean $^{87}Sr/^{86}Sr_{sw}$ of preceding 200 Ma
Hydrothermal input flux	$F(Sr)_{hyd\text{-}in}$	$\delta^{88/86}Sr_{hyd\text{-}in}$ = 0.27‰ [c]	$^{87}Sr/^{86}Sr_{hyd\text{-}in}$ = 0.7025 [e]
Alteration flux into the oceanic crust	$F(Sr)_{alt}$	$\Delta^{88/86}Sr_{alt\text{-}sw}$ = -0.01‰ [d]	$^{87}Sr/^{86}Sr_{alt}$ = $^{87}Sr/^{86}Sr_{sw}$
Carbonate-related net flux	$F(Sr)_{carb}$	$\Delta^{88/86}Sr_{carb\text{-}sw}$ = -0.24‰	$^{87}Sr/^{86}Sr_{carb}$ = $^{87}Sr/^{86}Sr_{sw}$

[a] Calculated from a 1:1 mixture of basalts (0.25‰ (Moynier et al., 2010)) and granites (0.295‰ (Ohno and Hirata, 2007)) assuming no isotope fraction during weathering processes. [b] The isotopic composition of the silicate continental weathering flux through geological time depends on spreading rates at MOR and continental erosion rates which have different effects on weathering of basaltic ($^{87}Sr/^{86}Sr$ = 0.705) and non-basaltic ($^{87}Sr/^{86}Sr$ = 0.712) rocks (see basic model from Wallmann (2004) for details). [a] Due to the similarity in the $^{87}Sr/^{86}Sr$ ratio of groundwater (0.7110) and continental river discharge (0.7119) (Basu et al., 2001; Palmer and Edmond, 1989), these fluxes are combined in our numerical model (Farkaš et al., 2007; Wallmann, 2001). Data from [c] (Charlier et al., 2012; Krabbenhöft et al., 2010), [d] (Böhm et al., 2012), and [e] (Davis et al., 2003).

6.2 Figure captions

Figure caption 1 - $\delta^{88/86}Sr$ measured in modern brachiopods. Within the external reproducibility of our method (±0.022‰ 2 s.d.), $\delta^{88/86}Sr$ is found to be independent of habitat location (Triangles = North Atlantic, squares = Pacific, circle = Mediterranean Sea), species, and water temperature with a mean of 0.176±0.016‰ (black line with 2 s.d. of the mean (dashed line), n=13, table A3 in the electronic annex).

Figure caption 2 - $\delta^{88/86}Sr$ of marine carbonates ($\delta^{88/86}Sr_{cc}$) through geological time (Triangles = brachiopods, diamonds = belemnites, squares = carbonate matrices). Open symbols represent unreliable samples according to our selection criteria. Closed symbols represent reliable samples that are used to reconstruct seawater $\delta^{88/86}Sr$ (Fig. 3). Long-term external reproducibility (2 s.d.) of coral standard JCp-1 corresponds to ±0.022‰ (n=32). The horizontal black dashed line represents Phanerozoic mean $\delta^{88/86}Sr_{cc}$ of 0.16‰. Time scale and geological periods are from GTS 2012 (Gradstein et al., 2012). Abbreviations for geological periods: Cret = Cretaceous, Jura = Jurassic, Trias = Triassic, Perm = Permian, Carbon = Carboniferous, Devon = Devonian, Sil = Silurian, Ord = Ordovician, € = Cambrian. Coloring of periods follows the Commission for the Geological Map of the World (http://www.ccgm.org).

Figure caption 3 – The stable and radiogenic strontium and calcium isotope composition of Phanerozoic seawater. Red curve represents a 5Myr running mean

$\delta^{88/86}Sr_{sw}$ record reconstructed from brachiopods and belemnites (Fig. 2). Dashed line represents an interpolation of $\delta^{88/86}Sr_{sw}$ data points in the Late Triassic and Late Jurassic (see section 4.2 for details). Green curve represents $(^{87}Sr/^{86}Sr)_{sw}$ data compiled by McArthur et al. (2001) (Look-Up Table Version 4: 08/ 04). Blue curve represents a 10Myr running mean through the $\delta^{44/40}Ca_{sw}$ (vs. SRM915a) data of (Farkaš et al., 2007a). Blue and red dashed-dotted horizontal lines represent the isotope composition of mantle derived Ca and Sr sources, respectively (Huang et al., 2010; Krabbenhöft et al., 2010). Red, green, and blue stars represent modern seawater isotope ratios for $\delta^{88/86}Sr$, $^{87}Sr/^{86}Sr$, and $\delta^{44/40}Ca$, respectively (Hippler et al., 2003; Krabbenhöft et al., 2009; McArthur, 1994). Grey vertical bars represent 50Myr time intervals and are for easing comparison between isotope curves. Time scale and geological periods from GTS 2012 (Gradstein et al., 2012). Abbreviations for geological periods are the same as in figure caption 2.

Figure caption 4 – Model scheme for the marine Sr budget. Changes in seawater Sr concentrations and isotope compositions depend on changes in the fluxes of silicate and carbonate continental weathering ($F(Sr)_{ws}$ and $F(Sr)_{wc}$), hydrothermal input ($F(Sr)_{hyd\text{-}in}$), alteration of the oceanic crust ($F(Sr)_{alt}$), and the carbonate-related net flux ($F(Sr)_{carb}$), consisting of carbonate dissolution and carbonate burial fluxes.

Figure caption 5 – Modeled Sr fluxes (all in 10^{10}mol/yr) and seawater Sr concentration (in µmol/l). Negative $F(Sr)_{carb}$ correspond to a net output of Sr out of the ocean while positive $F(Sr)_{carb}$ values correspond to a net input of Sr from carbonate dissolution to the ocean. Dashed line represents the time interval of missing $\delta^{88/86}Sr_{sw}$ input data (see figure caption 3 and section 4.2 for details).

Figure caption 6 – Modeled $(Sr/Ca)_{sw}$ ratios and $D(F)_{Sr}$ during the Phanerozoic Eon are shown together with literature data. Upper part: Modeled $(Sr/Ca)_{sw}$ ratios (solid and dashed black line; see figure caption 3 and section 4.2 for details) show a general agreement with published $(Sr/Ca)_{sw}$ ratios (three point running mean of Steuber and Veizer (2002); orange line with 2 s.d. (dashed orange line)). Lower part: Modeled $D(F)_{Sr}$ (see text for definition) and end member partition coefficients for aragonite ($D_{Sr} \approx 1$) and calcite ($D_{Sr} \approx 0.1$) (dashed-dotted horizontal lines). Time

periods of proposed “aragonite” and “calcite” seas are from (Stanley and Hardie, 1998).

Figure caption 7 – Modeled carbonate related Sr net flux ($F(Sr)_{carb}$, solid and dashed black line; see figure caption 3 and section 4.2 for details) is shown together with sea level changes (blue line) and intervals of glaciations (blue bars at the top) and ocean anoxia (black bars at the bottom). Note that negative $F(Sr)_{carb}$ indicate Sr carbonate burial fluxes exceeding Sr carbonate dissolution fluxes and vice versa. Times of positive $F(Sr)_{carb}$ ($>0.5x10^{10}$mol/yr, marked by light blue vertical bars) correlate in 5 of 6 cases (2 x Ordovician, Silurian, Carboniferous, and Permian period) with glacial intervals. Times of highly negative $F(Sr)_{carb}$ and therefore high carbonate burial (marked by grey vertical bars) correlate in 2 of 3 cases (Permian/Triassic transition and Cretaceous period) with times of ocean anoxia. Sea level and Paleozoic intervals of anoxia and glacials are from (Giles, 2012; Haq et al., 1987; Haq and Schutter, 2008). Mesozoic glacial intervals are from (Price, 1999). Mesozoic anoxic intervals are from (Erba, 2004). Timing of the P/T anoxia are from (Isozaki, 1997). Time scale and geological periods are from GTS 2012 (Gradstein et al., 2012). PD = present day, N = Neogene, P = Paleogene. Other abbreviations for geological periods are the same as in figure caption 2.

Figure caption 8 - Modeled marine Sr budget in the Permian and Triassic period. Modeled $F(Sr)_{carb}$ is represented by the blue shaded area and modelled Sr_{sw} concentration by the solid black curve. Note that negative $F(Sr)_{carb}$ indicate Sr carbonate burial fluxes exceeding Sr carbonate dissolution fluxes and vice versa. Modelled period of high carbonate burial from ~260Ma to ~245Ma coincides with the period of increasing long-term $\delta^{34}S_{CAS}$ values (red curve) (Kampschulte and Strauss, 2004) and periods of stratified and superanoxic ocean conditions as defined by (Isozaki, 1997). The grey box represents the time of high particulate organic carbon burial (POC) after (Berner and Canfield, 1989). The P/T boundary is marked by a vertical dashed line at 251Ma. Time scale and stratigraphic stages are from (Ogg et al., 2008). As = Asselian, Sak = Sakmarian, Artinsk = Artinskian, Ku = Kungurian, R = Roadian, W = Wordian, Cap = Capitanian, Wuc = Wuchiapingian, C = Changhsingian, I = Induan, Ol = Olenekian, Anis = Anisian, Ladin = Ladinian, Rh = Rhaetian.

Figure caption 9 – Modeled Sr residence time in the ocean (τ_{Sr}, solid and dashed-dotted black lines and grey shaded area) and rate of change in seawater $^{88}Sr/^{86}Sr$ (solid and dashed red line; see figure caption 3 for details) and $^{87}Sr/^{86}Sr$ (green line, calculated from (McArthur et al., 2001). The periods with the highest rates of change are observed during periods of relatively short marine Sr residence times and indicated by light red and green bars for $\delta^{88/86}Sr_{sw}$ and $(^{87}Sr/^{86}Sr)_{sw}$, respectively. True τ_{Sr} (grey shaded area) lies in between τ_{Sr} calculated from Sr input fluxes (dashed-dotted line) and output fluxes (solid line).$\tau_{Sr} = M(Sr)_{sw} / \sum F(Sr)_{input}$ or = $M(Sr)_{sw} / \sum F(Sr)_{output}$, respectively, where $M(Sr)_{sw}$ is moles of Sr in seawater and $\sum F(Sr)_{input}$ and $\sum F(Sr)_{output}$ are the sums of input and output fluxes in mol/Myr, respectively (see section 4.2 for details). Time scale and geological periods are from (Gradstein et al., 2012). Abbreviations for geological periods are the same as in figure caption 2 and 7.

7 Acknowledgements

Financial support: DFG, Ei272/29-1 (QUASAR); CIFAR-ESEP; GACR grant (P210/12/P631). We thank A. Kolevica, F. Hauff, A. Rüggeberg and K. Hissmann, B. Hansen, N. Nolte, P. Wickham, and E. Hathorne. The suggestions of two anonymous greatly helped to improve the manuscript.

8 Literature

Allègre, C.J., Louvat, P., Gaillardet, J., Meynadier, L., Rad, S., Capmas, F., 2010. The fundamental role of island arc weathering in the oceanic Sr isotope budget. Earth Planet. Sci. Lett. 292, 51-56.

Artemov, Y.M., Strizhov, V.P., Ustinov, V.I., Yaroshevskiy, A.A., 1967. Possible isotope fractionation during dolomitization (in russian). Geokhimiya 5, 519-529.

Azmy, K., Veizer, J., Bassett, M.G., Copper, P., 1998. Oxygen and carbon isotopic composition of Silurian brachiopods: Implications for coeval seawater and glaciations. Geol. Soc. Am. Bull. 110, 1499-1512.

Banner, J.L., Hanson, G.N., 1990. Calculation of simultaneous isotopic and trace element variations during water-rock interaction with applications to carbonate diagenesis. Geochim. Cosmochim. Acta 54, 3123-3137.

Basu, A.R., Jacobsen, S.B., Poreda, R.J., Dowling, C.B., Aggarwal, P.K., 2001. Large Groundwater Strontium Flux to the Oceans from the Bengal Basin and the Marine Strontium Isotope Record. Science 293, 1470-1473.

Berner, E.K., Berner, R.A., 2012. Global environment : water, air, and geochemical cycles, 2 ed. Princeton University Press.

Berner, R.A., 1994. GEOCARB II; a revised model of atmospheric CO_2 over Phanerozoic time. Am J Sci 294, 56-91.

Berner, R.A., Canfield, D.E., 1989. A new model for atmospheric oxygen over Phanerozoic time. Am J Sci 289, 333-361.

Blättler, C.L., Henderson, G.M., Jenkyns, H.C., 2012. Explaining the Phanerozoic Ca isotope history of seawater. Geology 40, 843-846.

Blum, J.D., Erel, Y., 1997. Rb-Sr isotope systematics of a granitic soil chronosequence: The importance of biotite weathering. Geochim. Cosmochim. Acta 61, 3193-3204.

Böhm, F., Eisenhauer, A., Tang, J., Dietzel, M., Krabbenhöft, A., Kisakürek, B., Horn, C., 2012. Strontium isotope fractionation of planktic foraminifera and inorganic calcite. Geochim. Cosmochim. Acta.

Brand, U., Logan, A., Hiller, N., Richardson, J., 2003. Geochemistry of modern brachiopods: applications and implications for oceanography and paleoceanography. Chem. Geol. 198, 305-334.

Brennecka, G.A., Herrmann, A.D., Algeo, T.J., Anbar, A.D., 2011. Rapid expansion of oceanic anoxia immediately before the end-Permian mass extinction. Proceedings of the National Academy of Sciences 108, 17631-17634.

Bruckschen, P., Oesmann, S., Veizer, J., 1999. Isotope stratigraphy of the European Carboniferous: proxy signals for ocean chemistry, climate and tectonics. Chem. Geol. 161, 127-163.

Bruhn, F., Bruckschen, P., Richter, D.K., Meijer, J., Stephan, A., Veizer, J., 1995. Diagenetic History of Sedimentary Carbonates - Constraints from Combined Cathodoluminescence and Trace-Element Analyses by Micro-Pixe. Nucl. Instrum. Methods Phys. Res. Sect. B-Beam Interact. Mater. Atoms 104, 409-414.

Butterfield, D.A., Nelson, B.K., Wheat, C.G., Mottl, M.J., Roe, K.K., 2001. Evidence for basaltic Sr in midocean ridge-flank hydrothermal systems and implications for the global oceanic Sr isotope balance. Geochim. Cosmochim. Acta 65, 4141-4153.

Charlier, B.L.A., Nowell, G.M., Parkinson, I.J., Kelley, S.P., Pearson, D.G., Burton, K.W., 2012. High temperature strontium stable isotope behaviour in the early solar system and planetary bodies. Earth Planet. Sci. Lett. 329-330, 31-40.

Chen, Z.-Q., Benton, M.J., 2012. The timing and pattern of biotic recovery following the end-Permian mass extinction. Nature Geosci 5, 375-383.

Davis, A.C., Bickle, M.J., Teagle, D.A.H., 2003. Imbalance in the oceanic strontium budget. Earth Planet. Sci. Lett. 211, 173-187.

Derry, L.A., 2009. Geochemistry: A glacial hangover. Nature 458, 417-418.

Diener, A., Ebneth, S., Veizer, J., Buhl, D., 1996. Strontium isotope stratigraphy of the Middle Devonian: Brachiopods and conodonts. Geochim. Cosmochim. Acta 60, 639-652.

Drever, J.I., 1997. The Geochemistry of Natural Waters: Surface and Groundwater Environments, 3rd edition ed. Pearson Education.

Dromgoole, E.L., Walter, L.M., 1990. Iron and manganese incorporation into calcite: Effects of growth kinetics, temperature and solution chemistry. Chem. Geol. 81, 311-336.

Eisenhauer, A., Böhm, F., Vollstaedt, H., Krabbenhöft, A., Liebetrau, V., Fietzke, J., Kisakürek, B., Erez, J., 2011. Strontium isotope fractionation and its application in earth system sciences Goldschmidt 2011, Prague, Czech Republic.

Erba, E., 2004. Calcareous nannofossils and Mesozoic oceanic anoxic events. Marine Micropaleontology 52, 85-106.

Farkaš, J., Böhm, F., Wallmann, K., Blenkinsop, J., Eisenhauer, A., van Geldern, R., Munnecke, A., Voigt, S., Veizer, J., 2007a. Calcium isotope record of Phanerozoic oceans: Implications for chemical evolution of seawater and its causative mechanisms. Geochim. Cosmochim. Acta 71, 5117-5134.

Farkaš, J., Buhl, D., Blenkinsop, J., Veizer, J., 2007b. Evolution of the oceanic calcium cycle during the late Mesozoic: Evidence from $\delta^{44/40}$Ca of marine skeletal carbonates. Earth Planet. Sci. Lett. 253, 96-111.

Farkaš, J., Chakrabarti, R., Jacobsen, S.B., Kump, L.R., Melezhik, V.A., 2013. 7.10 Chemical Characteristics of Sediments and Seawater, in: Melezhik, V.A., Prave, A.R., Hanski, E.J., Fallick, A.E., Lepland, A., Kump, L.R., Strauss, H. (Eds.), Reading the Archive of Earth's Oxygenation. Springer Berlin Heidelberg, pp. 1457-1514.

Fietzke, J., Eisenhauer, A., 2006. Determination of temperature-dependent stable strontium isotope (^{88}Sr/^{86}Sr) fractionation via bracketing standard MC-ICP-MS. Geochem. Geophys. Geosyst. 7, Q08009.

Gaillardet, J., Dupré, B., Louvat, P., Allègre, C.J., 1999. Global silicate weathering and CO_2 consumption rates deduced from the chemistry of large rivers. Chem. Geol. 159, 3-30.

Giles, P.S., 2012. Low-latitude Ordovician to Triassic brachiopod habitat temperatures (BHTs) determined from δ^{18}O[brachiopod calcite]: A cold hard look at ice-house tropical oceans. Palaeogeography, Palaeoclimatology, Palaeoecology 317–318, 134-152.

Gorjan, P., Kaiho, K., 2007. Correlation and comparison of seawater $\delta^{34}S_{CAS}$ records at the Permian-Triassic transition. Chem. Geol. 243, 275-285.

Gradstein, F.M., Ogg, J.G., Schmitz, M., Ogg, G., 2012. The Geologic Time Scale 2012, 1 ed. Elsevier.

Grotzinger, J.P., Knoll, A.H., 1995. Anomalous carbonate precipitates; is the Precambrian the key to the Permian? Palaios 10, 578-596.

Gussone, N., Böhm, F., Eisenhauer, A., Dietzel, M., Heuser, A., Teichert, B.M.A., Reitner, J., Wörheide, G., Dullo, W.-C., 2005. Calcium isotope fractionation in calcite and aragonite. Geochim. Cosmochim. Acta 69, 4485-4494.

Haq, B.U., Hardenbol, J., Vail, P.R., 1987. Chronology of Fluctuating Sea Levels Since the Triassic. Science 235, 1156-1167.

Haq, B.U., Schutter, S.R., 2008. A chronology of Paleozoic sea-level changes. Science 322, 64-68.

Hardie, L.A., 1996. Secular variation in seawater chemistry: An explanation for the coupled secular variation in the mineralogies of marine limestones and potash evaporites over the past 600 m.y. Geology 24, 279-283.

Hinojosa, J.L., Brown, S.T., Chen, J., DePaolo, D.J., Paytan, A., Shen, S.-z., Payne, J.L., 2012. Evidence for end-Permian ocean acidification from calcium isotopes in biogenic apatite. Geology.

Hippler, D., Schmitt, A.-D., Gussone, N., Heuser, A., Stille, P., Eisenhauer, A., Nägler, T.F., 2003. Calcium Isotopic Composition of Various Reference Materials and Seawater. Geostandards Newsletter 27, 13-19.

Hodell, D.A., Mead, G.A., Mueller, P.A., 1990. Variation in the strontium isotopic composition of seawater (8 Ma to present) : Implications for chemical weathering rates and dissolved fluxes to the oceans. Chemical Geology: Isotope Geoscience section 80, 291-307.

Hodell, D.A., Mueller, P.A., McKenzie, J.A., Mead, G.A., 1989. Strontium isotope stratigraphy and geochemistry of the late Neogene ocean. Earth Planet. Sci. Lett. 92, 165-178.

Holmden, C., 2009. Ca isotope study of Ordovician dolomite, limestone, and anhydrite in the Williston Basin: Implications for subsurface dolomitization and local Ca cycling. Chem. Geol. 268, 180-188.

Holmden, C., Papanastassiou, D.A., Blanchon, P., Evans, S., 2012. $\delta^{44/40}$Ca variability in shallow water carbonates and the impact of submarine groundwater discharge on Ca-cycling in marine environments. Geochim. Cosmochim. Acta 83, 179-194.

Horita, J., Zimmermann, H., Holland, H.D., 2002. Chemical evolution of seawater during the Phanerozoic: Implications from the record of marine evaporites. Geochim. Cosmochim. Acta 66, 3733-3756.

Huang, S., Farkaš, J., Jacobsen, S.B., 2010. Calcium isotopic fractionation between clinopyroxene and orthopyroxene from mantle peridotites. Earth Planet. Sci. Lett. 292, 337-344.

Isozaki, Y., 1997. Permo-Triassic boundary superanoxia and stratified superocean: Records from lost deep sea. Science 276, 235-238.

Jenkyns, H.C., 2010. Geochemistry of oceanic anoxic events. Geochem. Geophys. Geosyst. 11, Q03004.

Jones, C.E., Jenkyns, H.C., Coe, A.L., Stephen, H.P., 1994a. Strontium isotopic variations in Jurassic and Cretaceous seawater. Geochim. Cosmochim. Acta 58, 3061-3074.

Jones, C.E., Jenkyns, H.C., Hesselbo, S.P., 1994b. Strontium isotopes in Early Jurassic seawater. Geochim. Cosmochim. Acta 58, 1285-1301.

Jones, M.T., Pearce, C.R., Jeandel, C., Gislason, S.R., Eiriksdottir, E.S., Mavromatis, V., Oelkers, E.H., 2013. Riverine particulate material dissolution as a significant flux of strontium to the oceans. Earth Planet. Sci. Lett. 355â€“356, 51-59.

Kaiho, K., Kajiwara, Y., Chen, Z.-Q., Gorjan, P., 2006. A sulfur isotope event at the end of the Permian. Chem. Geol. 235, 33-47.

Kampschulte, A., Strauss, H., 2004. The sulfur isotopic evolution of Phanerozoic seawater based on the analysis of structurally substituted sulfate in carbonates. Chem. Geol. 204, 255-286.

Kershaw, S., Crasquin, S., Li, Y., Collin, P.Y., Forel, M.B., Mu, X., Baud, A., Wang, Y., Xie, S., Maurer, F., Guo, L., 2011. Microbialites and global environmental change across the Permian–Triassic boundary: a synthesis. Geobiology 10, 25-47.

Knoll, A.H., Bambach, R.K., Canfield, D.E., Grotzinger, J.P., 1996. Comparative earth history and Late Permian mass extinction. Science 273, 452-457.

Korte, C., Jasper, T., Kozur, H.W., Veizer, J., 2006. $^{87}Sr/^{86}Sr$ record of Permian seawater. Palaeogeography, Palaeoclimatology, Palaeoecology 240, 89-107.

Korte, C., Kozur, H.W., Veizer, J., 2005. $\delta^{13}C$ and $\delta^{18}O$ values of Triassic brachiopods and carbonate rocks as proxies for coeval seawater and palaeotemperature. Palaeogeography, Palaeoclimatology, Palaeoecology 226, 287-306.

Kothavala, Z., Oglesby, R.J., Saltzman, B., 1999. Sensitivity of equilibrium surface temperature of CCM3 to systematic changes in atmospheric CO_2. Geophys Res Lett 26, 209-212.

Krabbenhöft, A., Eisenhauer, A., Böhm, F., Vollstaedt, H., Fietzke, J., Liebetrau, V., Augustin, N., Peucker-Ehrenbrink, B., Hansen, B.T., Nolte, N., Wallmann, K., 2010. Constraining the marine strontium budget with natural strontium isotope fractionations ($^{87}Sr/^{86}Sr^*$-$\delta^{88/86}Sr$) of carbonates, hydrothermal solutions and river waters. Geochim. Cosmochim. Acta 74, 4097-4109.

Krabbenhöft, A., Fietzke, J., Eisenhauer, A., Liebetrau, V., Böhm, F., Vollstaedt, H., 2009. Determination of radiogenic and stable strontium isotope ratios ($^{87}Sr/^{86}Sr$; $\delta^{88/86}Sr$) by thermal ionization mass spectrometry applying an $^{87}Sr/^{84}Sr$ double spike. J. Anal. At. Spectrom. 24, 1267-1271.

Krause, S., Liebetrau, V., Gorb, S., Sánchez-Román, M., McKenzie, J.A., Treude, T., 2012. Microbial nucleation of Mg-rich dolomite in exopolymeric substances under anoxic modern seawater salinity: New insight into an old enigma. Geology 40, 587-590.

Lepzelter, C.G., Anderson, T.F., Sandberg, P.A., 1983. Stable isotope variations in modern articulate brachiopods. AAPG Bull.-Am. Assoc. Petr. Geol. 67, 500-501.

Lowenstein, T.K., Timofeeff, M.N., Kovalevych, V.M., Horita, J., 2005. The major-ion composition of Permian seawater. Geochim. Cosmochim. Acta 69, 1701-1719.

Luo, G., Kump, L.R., Wang, Y., Tong, J., Arthur, M.A., Yang, H., Huang, J., Yin, H., Xie, S., 2010. Isotopic evidence for an anomalously low oceanic sulfate concentration following end-Permian mass extinction. Earth Planet. Sci. Lett. 300, 101-111.

McArthur, J.M., 1994. Recent Trends in Strontium Isotope Stratigraphy. Terr. Nova 6, 331-358.

McArthur, J.M., Howarth, R.J., Bailey, T.R., 2001. Strontium Isotope Stratigraphy: LOWESS version 3: Best fit to the marine Sr-isotope curve for 0-509 Ma and accompanying look-up table for deriving numerical age. The Journal of Geology 109, 155-170.

Milliman, J.D., Müller, G., Förstner, U., 1974. Recent sedimentary carbonates Springer Verlag, New York, Heidelberg, Berlin.

Morrison, J.O., Brand, U., 1988. An evaluation of diagenesis and chemostratigraphy of upper cretaceous molluscs from the Canadian Interior Seaway. Chemical Geology: Isotope Geoscience section 72, 235-248.

Morse, J.W., Wang, Q., Tsio, M.Y., 1997. Influences of temperature and Mg:Ca ratio on CaCO3 precipitates from seawater. Geology 25, 85-87.

Moynier, F., Agranier, A., Hezel, D.C., Bouvier, A., 2010. Sr stable isotope composition of Earth, the Moon, Mars, Vesta and meteorites. Earth Planet. Sci. Lett. 300, 359-366.

Nägler, T.F., Eisenhauer, A., Müller, A., Hemleben, C., Kramers, J., 2000. The δ^{44}Ca-temperature calibration on fossil and cultured Globigerinoides sacculifer: New tool for reconstruction of past sea surface temperatures. Geochem. Geophys. Geosyst. 1.

Newton, R.J., Pevitt, E.L., Wignall, P.B., Bottrell, S.H., 2004. Large shifts in the isotopic composition of seawater sulphate across the Permo-Triassic boundary in northern Italy. Earth Planet. Sci. Lett. 218, 331-345.

Nier, A.O., 1938. The Isotopic Constitution of Strontium, Barium, Bismuth, Thallium and Mercury. Physical Review 54, 275.

Ohno, T., Hirata, T., 2007. Simultaneous determination of mass-dependent isotopic fractionation and radiogenic isotope variation of strontium in geochemical samples by Multiple Collector-ICP-Mass Spectrometry. Anal. Sci. 23, 1275-1280.

Okai, T., Suzuki, A., Kawahata, H., Terashima, S., Imai, N., 2002. Preparation of a New Geological Survey of Japan Geochemical Reference Material: Coral JCp-1. Geostandards Newsletter 26, 95-99.

Palmer, M.R., Edmond, J.M., 1989. The strontium isotope budget of the modern ocean. Earth Planet. Sci. Lett. 92, 11-26.

Payne, J.L., Clapham, M.E., 2012. End-Permian Mass Extinction in the Oceans: An Ancient Analog for the Twenty-First Century? Annu. Rev. Earth Planet. Sci. 40, 89-111.

Payne, J.L., Turchyn, A.V., Paytan, A., DePaolo, D.J., Lehrmann, D.J., Yu, M., Wei, J., 2010. Calcium isotope constraints on the end-Permian mass extinction. Proceedings of the National Academy of Sciences 107, 8543-8548.

Porder, S., Hilley, G.E., Chadwick, O.A., 2007. Chemical weathering, mass loss, and dust inputs across a climate by time matrix in the Hawaiian Islands. Earth Planet. Sci. Lett. 258, 414-427.

Price, G.D., 1999. The evidence and implications of polar ice during the Mesozoic. Earth-Science Reviews 48, 183-210.

Prokoph, A., Shields, G.A., Veizer, J., 2008. Compilation and time-series analysis of a marine carbonate $\delta^{18}O$, $\delta^{13}C$, $^{87}Sr/^{86}Sr$ and $\delta^{34}S$ database through Earth history. Earth-Science Reviews 87, 113-133.

Raddatz, J., Liebetrau, V., Rüggeberg, A., Hathorne, E., Krabbenhöft, A., Eisenhauer, A., Böhm, F., Vollstaedt, H., Fietzke, J., López Correa, M., Freiwald, A., Dullo, W.C., 2013. Stable Sr-isotope, Sr/Ca, Mg/Ca, Li/Ca and Mg/Li ratios in the scleractinian cold-water coral Lophelia pertusa. Chem. Geol. 352, 143-152.

Richter, F.M., DePaolo, D.J., 1988. Diagenesis and Sr isotopic evolution of seawater using data from DSDP 590B and 575. Earth Planet. Sci. Lett. 90, 382-394.

Richter, F.M., Rowley, D.B., DePaolo, D.J., 1992. Sr isotope evolution of seawater: the role of tectonics. Earth Planet. Sci. Lett. 109, 11-23.

Riding, R., Liang, L., 2005. Geobiology of microbial carbonates: metazoan and seawater saturation state influences on secular trends during the Phanerozoic. Palaeogeography, Palaeoclimatology, Palaeoecology 219, 101-115.

Riebesell, U., Wolf-Gladrow, D.A., Smetacek, V., 1993. Carbon dioxide limitation of marine phytoplankton growth rates. Nature 361, 249-251.

Sandberg, P.A., 1983. An oscillating trend in Phanerozoic non-skeletal carbonate mineralogy. Nature 305, 19-22.

Smalley, P.C., Higgins, A.C., Howarth, R.J., Nicholson, H., Jones, C.E., Swinburne, N.H.M., Bessa, J., 1994. Seawater Sr Isotope Variations through Time - a Procedure for Constructing a Reference Curve to Date and Correlate Marine Sedimentary-Rocks. Geology 22, 431-434.

Sobolev, S.V., Sobolev, A.V., Kuzmin, D.V., Krivolutskaya, N.A., Petrunin, A.G., Arndt, N.T., Radko, V.A., Vasiliev, Y.R., 2011. Linking mantle plumes, large igneous provinces and environmental catastrophes. Nature 477, 312-316.

Souza, G.F.d., Reynolds, B.C., Kiczka, M., Bourdon, B., 2010. Evidence for mass-dependent isotopic fractionation of strontium in a glaciated granitic watershed. Geochim. Cosmochim. Acta 74, 2596-2614.

Spooner, E.T.C., 1976. The strontium isotopic composition of seawater, and seawater-oceanic crust interaction. Earth Planet. Sci. Lett. 31, 167-174.

Stanley, S.M., Hardie, L.A., 1998. Secular oscillations in the carbonate mineralogy of reef-building and sediment-producing organisms driven by tectonically forced shifts in seawater chemistry. Palaeogeography, Palaeoclimatology, Palaeoecology 144, 3-19.

Steuber, T., Veizer, J., 2002. Phanerozoic record of plate tectonic control of seawater chemistry and carbonate sedimentation. Geology 30, 1123-1126.

Stoll, H.M., Schrag, D.P., 1998. Effects of Quaternary sea level cycles on strontium in seawater. Geochim. Cosmochim. Acta 62, 1107-1118.

Strauss, H., 1997. The isotopic composition of sedimentary sulfur through time. Palaeogeography, Palaeoclimatology, Palaeoecology 132, 97-118.

Taylor, A., Blum, J.D., 1995. Relation between soil age and silicate weathering rates determined from the chemical evolution of a glacial chronosequence. Geology 23, 979-982.

Vance, D., Teagle, D.A.H., Foster, G.L., 2009. Variable Quaternary chemical weathering fluxes and imbalances in marine geochemical budgets. Nature 458, 493-496.

Veizer, J., 1988. The earth and its life: Systems perspective. Origins of Life and Evolution of Biospheres 18, 13-39.

Veizer, J., 1989. Strontium Isotopes in Seawater through Time. Annu. Rev. Earth Planet. Sci. 17, 141-167.

Veizer, J., Ala, D., Azmy, K., Bruckschen, P., Buhl, D., Bruhn, F., Carden, G.A.F., Diener, A., Ebneth, S., Godderis, Y., Jasper, T., Korte, C., Pawellek, F., Podlaha, O.G., Strauss, H., 1999. $^{87}Sr/^{86}Sr$, $\delta^{13}C$ and $\delta^{18}O$ evolution of Phanerozoic seawater. Chem. Geol. 161, 59-88.

Veizer, J., Bruckschen, P., Pawellek, F., Diener, A., Podlaha, O.G., Carden, G.A.F., Jasper, T., Korte, C., Strauss, H., Azmy, K., Ala, D., 1997a. Oxygen isotope evolution of Phanerozoic seawater. Paleogeogr. Paleoclimatol. Paleoecol. 132, 159-172.

Veizer, J., Buhl, D., Diener, A., Ebneth, S., Podlaha, O.G., Bruckschen, P., Jasper, T., Korte, C., Schaaf, M., Ala, D., Azmy, K., 1997b. Strontium isotope stratigraphy: potential resolution and event correlation. Paleogeogr. Paleoclimatol. Paleoecol. 132, 65-77.

Veizer, J., Compston, W., Clauer, N., Schidlowski, M., 1983. in Late Proterozoic carbonates: evidence for a "mantle" event at ~900 Ma ago. Geochim. Cosmochim. Acta 47, 295-302.

Veizer, J., Mackenzie, F.T., 2010. Evolution of Sedimentary Rocks, in: Holland, H.D., Turekian, K.K. (Eds.), Readings from the Treatise of Geochemistry. Elsevier, pp. 467-506.

Wallmann, K., 2001. Controls on the cretaceous and cenozoic evolution of seawater composition, atmospheric CO_2 and climate. Geochim. Cosmochim. Acta 65, 3005-3025.

Wallmann, K., 2004. Impact of atmospheric CO_2 and galactic cosmic radiation on Phanerozoic climate change and the marine $\delta^{18}O$ record. Geochem. Geophys. Geosyst. 5.

White, A.F., Brantley, S.L., 2003. The effect of time on the weathering of silicate minerals: why do weathering rates differ in the laboratory and field? Chem. Geol. 202, 479-506.

Wignall, P.B., 2007. The End-Permian mass extinction – how bad did it get? Geobiology 5, 303-309.

Wignall, P.B., Twitchett, R.J., 2002. Extent, duration, and nature of the Permian-Triassic superanoxic event. Geological Society of America Special Papers 356, 395-413.

Woods, A.D., Bottjer, D.J., Mutti, M., Morrison, J., 1999. Lower Triassic large sea-floor carbonate cements: Their origin and a mechanism for the prolonged biotic recovery from the end-Permian mass extinction. Geology 27, 645-648.

Zeebe, R.E., Westbroek, P., 2003. A simple model for the CaCO3 saturation state of the ocean: The “Strangelove,” the “Neritan,” and the “Cretan” Ocean. Geochemistry, Geophysics, Geosystems 4.

Zhou, L., Gao, S., Chris, H., Corey, A., Xie, S., 2009. Preliminary Mo isotope data of Phanerozoic clastic sediments from the northern margin of the Yangtze block and its implication for paleoenvironmental conditions. Chinese Science Bulletin 54, 822-829.

Zhu, P., Macdougall, J.D., 1998. Calcium isotopes in the marine environment and the oceanic calcium cycle. Geochim. Cosmochim. Acta 62, 1691-1698.